ADVANCED ELECTRONIC MATERIALS
www.advelectronicmat.de

Controlling Defect Formation of Nanoscale AlN: Toward Efficient Current Conduction of Ultrawide-Bandgap Semiconductors

*Yuanpeng Wu, David A. Laleyan, Zihao Deng, Chihyo Ahn, Anthony F. Aiello, Ayush Pandey, Xianhe Liu, Ping Wang, Kai Sun, Elaheh Ahmadi, Yi Sun, Mackillo Kira, Pallab K. Bhattacharya, Emmanouil Kioupakis, and Zetian Mi**

Ultrawide-bandgap semiconductors such as AlN, BN, and diamond hold tremendous promise for high-efficiency deep-ultraviolet optoelectronics and high-power/frequency electronics, but their practical application has been limited by poor current conduction. Through a combined theoretical and experimental study, it is shown that a critical challenge can be addressed for AlN nanostructures by using N-rich epitaxy. Under N-rich conditions, the p-type Al-substitutional Mg-dopant formation energy is significantly reduced by 2 eV, whereas the formation energy for N-vacancy related compensating defects is increased by ≈3 eV, both of which are essential to achieve high hole concentrations of AlN. Detailed analysis of the current–voltage characteristics of AlN p-i-n diodes suggests that current conduction is dominated by hole-carrier tunneling at room temperature, which is directly related to the activation energy of Mg dopants. At high Mg concentrations, the dispersion of Mg acceptor energy levels leads to drastically reduced activation energy for a portion of Mg dopants, evidenced by the small tunneling energy of 67 meV, which explains the efficient current conduction and the very small turn-on voltage (≈5 V) for the diodes made of nanoscale AlN. This work shows that nanostructures can overcome the dopability challenges of ultrawide-bandgap semiconductors and significantly increase the efficiency of devices.

Ultrawide-bandgap semiconductors, including AlN, BN, and diamond, are critical for applications in next-generation high-power, high-frequency electronics, ultraviolet (UV) optoelectronics, high-power photonics, and quantum devices and systems.[1–10] Progress in these fields, however, has been severely limited by the lack of scalable substrate, the presence of large densities of defects, and the extremely poor current conduction.[3,11,12] Moreover, it has remained challenging to achieve a precise control of impurity incorporation and defect formation in these ultrawide-bandgap semiconductors, severely limiting their structural, electronic, optical, and quantum properties. For example, free hole concentrations of AlN, the material of choice of high-efficiency UV light emitting diodes (LEDs) for water purification and disinfection, can only be measured at $\approx 10^{10}$ cm^{-3} level at room temperature for epilayer structures,[1,13,14] which is more than seven orders of magnitude lower than what is commonly required ($\approx 10^{17}$–10^{19} cm^{-3}) for practical optoelectronic and electronic devices. Magnesium (Mg), the common p-type dopant of III-nitrides, has a prohibitively large activation energy E_A for AlN,[13,15] which results in negligible doping efficiency at room temperature. Moreover, during the epitaxy of Mg-doped AlN, the Fermi level is shifted toward the valence band edge,[16] significantly reducing the formation energy for nitrogen-vacancy as well as donor-like point defect and impurity incorporation, shown in **Figure 1**a, which compensates the presence of free holes[17,18] and further introduces various defect-related emissions.[14,15] Illustrated in Figure 1b is the calculated formation energy for N-vacancy, Al-vacancy, and Al-substitutional Mg dopant incorporation, as a function of Fermi level of AlN. Detailed theoretical calculation process is described in Section S1, Supporting Information.

Here we show, both theoretically and experimentally, that such fundamental material issues of AlN can be potentially addressed through nonequilibrium epitaxy of nanostructures. Dislocation-free semiconductor nanostructures not only enhance the performance and functionality of electronic, photonic, and quantum devices and systems, but also open a new paradigm for controlling the formation of defects and

Y. Wu, D. A. Laleyan, C. Ahn, A. F. Aiello, A. Pandey, Dr. X. Liu, Dr. P. Wang, Prof. E. Ahmadi, Dr. Y. Sun, Prof. M. Kira, Prof. P. K. Bhattacharya, Prof. Z. Mi
Department of Electrical Engineering and Computer Science
University of Michigan
Ann Arbor, MI 48109, USA
E-mail: ztmi@umich.edu

Z. Deng, Dr. K. Sun, Prof. E. Kioupakis
Department of Materials Science and Engineering
University of Michigan
Ann Arbor, MI 48109, USA

The ORCID identification number(s) for the author(s) of this article can be found under https://doi.org/10.1002/aelm.202000337.

DOI: 10.1002/aelm.202000337

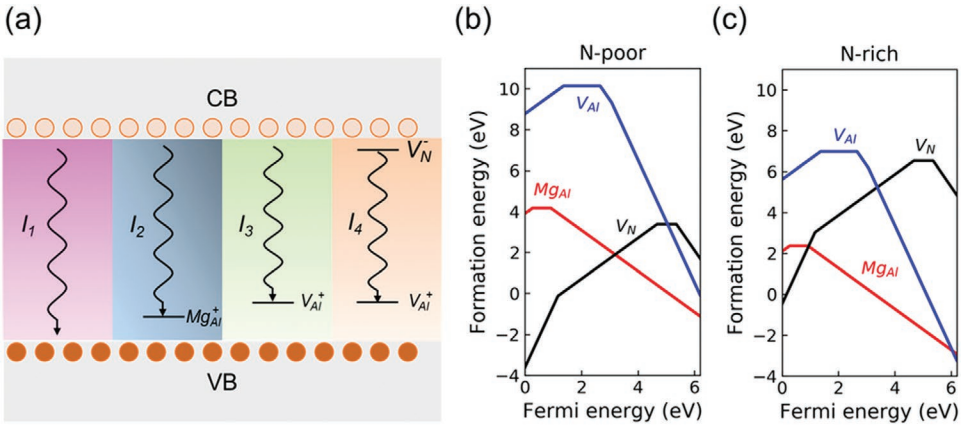

Figure 1. a) Illustration of various transitions in Mg-doped AlN that involve conduction band (CB), valence band (VB), Mg acceptors, Al-vacancies, and N-vacancies. b,c) Formation energies as a function of Fermi level for the nitrogen vacancy V_N, aluminum vacancy V_{Al}, and Al-substitutional Mg under N-poor and N-rich conditions. Fermi level is set to zero at the valence band maximum. The formation energy of N-vacancy related defects is increased by nearly 3 eV under N-rich epitaxy condition, compared to conventional N-poor condition. The formation energy for Al-substitutional Mg-dopant incorporation is decreased by ≈2 eV under N-rich epitaxy.

impurity incorporation.[19–24] During the epitaxy of N-polar AlN nanostructures, N-rich conditions are commonly used.[3,22,25] Illustrated in Figure 1c, the formation energy of N-vacancy related defects can be increased by nearly 3 eV under N-rich epitaxy condition, compared to conventional N-poor condition, thereby suppressing N-vacancy related defect formation. Moreover, the formation energy for Al-substitutional Mg-dopant incorporation is drastically reduced by ≈2 eV under N-rich epitaxy, shown in Figure 1c, which can significantly enhance Mg-dopant incorporation. Experimentally, we have studied optical properties of Mg-doped AlN nanostructures by deep-UV photoluminescence spectroscopy and their dependence on epitaxy conditions. Power-dependent and time-resolved photoluminescence measurements suggest that Mg-acceptor related optical emission originates from transitions between the conduction band and Mg impurity levels, rather than donor–acceptor pair (DAP) related emission measured in conventional AlN epilayers, indicating suppressed N-vacancy related defect formation. Detailed current-voltage (I–V) characteristics analysis of AlN p-i-n diodes suggests that current conduction is dominated by charge-carrier (hole) tunneling at room temperature, with the characteristic tunneling energy determined by the activation energy of the Mg dopant. The dispersion of Mg acceptor levels at very high concentrations leads to drastically reduced activation energy for a portion of Mg dopants, evidenced by a reduction of the characteristic tunneling energy from 364 to 67 meV. These studies provide a path for achieving efficient current conduction of AlN that is relevant for a broad range of deep-UV optoelectronic devices, including LEDs, lasers, photodetectors, modulators, as well as high-power and high-frequency transistors.

In this work, AlN nanostructures were grown on n-type Si wafer using a Veeco GEN II molecular beam epitaxy (MBE) system equipped with a radio frequency plasma-assisted nitrogen source. Shown in **Figure 2**a is the scanning electron microscopy (SEM) image. The grown nanowires have an average diameter of 50 nm and density of 1.5×10^{10} cm^{-2}, with an estimated filling factor of ≈30%. Listed in **Table 1**, AlN samples were grown under different conditions by varying N_2 flow rate, substrate temperature, and Mg flux (measured as beam equivalent pressure, BEP). The detailed growth process is described in the Experimental Section. All the samples were grown under N-rich epitaxy conditions and are largely free of dislocations and stacking faults (Figure S1, Supporting Information). For comparison, conventional AlN epilayers generally exhibit poor structural properties when grown under N-rich conditions.[26–28] While the suppression of N-vacancy related defects may be expected under N-rich epitaxy condition, its impact on the formation of other types of defects, such as Al vacancies, has remained unclear. In this study, we have first investigated the effect of growth temperature and N_2 flow rate on the properties of undoped AlN nanostructures. The studied samples, denoted as A1, A2, and A3, are listed in Table 1. Samples in Group A were grown in the temperature range of 810 °C to 965 °C with N_2 flow rates varying between 0.33 and 1 sccm.

Optical properties of AlN nanowires were measured using deep-UV photoluminescence spectroscopy (see the Experimental Section). As shown in Figure 2b, when grown under a N_2 flow rate of 1 sccm, Sample A1 (growth temperature of 965 °C) features a single excitonic emission peak at 5.93 eV (denoted as I_1), as expected for the excitonic emission of strain-free AlN.[29] An additional and broad Al vacancy related peak at 4.86 eV (denoted as I_3) was observed from Sample A2 (growth temperature of 810 °C), which is consistent with the calculated transition energy between conduction band and singly positive charged Al vacancy state (Figure S2a, Supporting Information). The comparison of the two spectra indicates that an elevated growth temperature helps suppress Al-vacancy related defect emission (I_3), through enhanced Al adatom diffusion.[30–32] In practical device applications, however, a relatively low growth temperature is generally required to enhance Mg dopant incorporation. Shown in Figure 1b,c, the formation energy for vacancies on Al site has a strong dependence on N chemical potentials, or N flux in the experiment. In this regard, Sample A3 was grown at 810 °C but with a relatively low N_2 flow rate of 0.33 sccm, yet maintaining N-rich epitaxy conditions. Shown

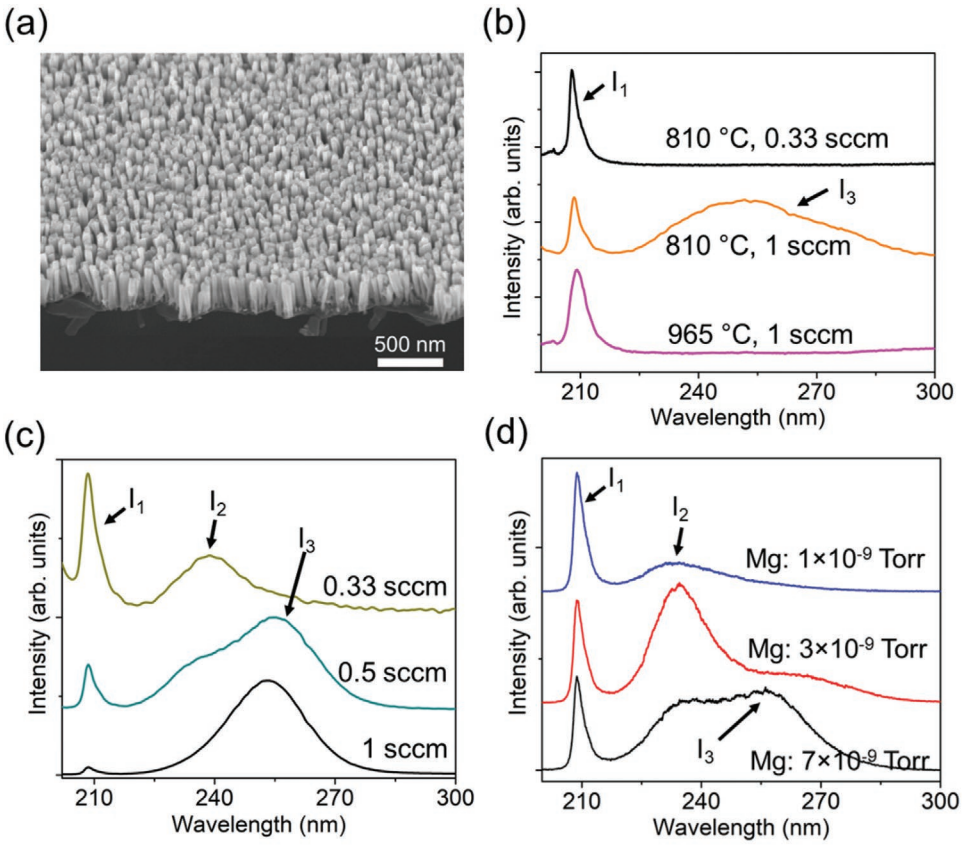

Figure 2. a) Scanning electron microscopy (SEM) image of AlN nanowires grown under 0.33 sccm nitrogen flow rate and substrate temperature of 810 °C. Scale bar, 500 nm. b) Normalized room-temperature photoluminescence spectra of undoped samples from Group A. Variations of the growth temperature and nitrogen flow rate are shown in the figure. c) Normalized photoluminescence spectra of Mg-doped samples from Group B. All samples were grown at a substrate temperature of 810 °C and Mg beam equivalent pressure (BEP) of 3×10^{-9} Torr while the nitrogen flow rate was varied among different samples. d) Normalized room-temperature photoluminescence spectra of Mg-doped samples from Group C. All samples were grown at a substrate temperature of 810 °C and N_2 flow rate of 0.4 sccm while Mg BEP was varied from 1×10^{-9} to 7×10^{-9} Torr.

in Figure 2b, Sample A3 features a strong excitonic emission (I_1) without defect-related emission (I_3), in spite of the relatively low growth temperature. Through these studies, it is evident that some of the commonly seen defects, including Al and N vacancies in AlN can be minimized by optimizing the growth parameters under N-rich epitaxy conditions.

Table 1. List of three groups of AlN samples presented in this work and their growth conditions including substrate temperature, N_2 flow rate, and Mg flux.

Sample label	Growth temperature [°C]	N_2 flow rate [sccm]	Mg flux [Torr]
A1	965	1	N.A.
A2	810	1	N.A.
A3	810	0.33	N.A.
B1	810	0.33	3×10^{-9}
B2	810	0.5	3×10^{-9}
B3	810	1	3×10^{-9}
C1	810	0.4	1×10^{-9}
C2	810	0.4	3×10^{-9}
C3	810	0.4	7×10^{-9}

In nanostructures, the complex growth dynamics, including surface adatom migration and desorption, may significantly affect the defect formation and distribution.[33,34] We have experimentally investigated the effect of Mg dopant incorporation on the defect formation. The studied samples (Group B) are listed in Table 1, which were grown at the same substrate temperature of 810 °C, but with N_2 flow rates varying from 0.33 to 1 sccm. Shown in Figure 2c, Mg-acceptor related emission (I_2) was clearly observed from Mg-doped AlN sample grown at a N_2 flow rate of 0.33 sccm, with negligible Al-vacancy related defect emission (I_3). The origin of I_2 can be attributed to transition between conduction band and singly positive charged Mg dopant state (Figure S2b, Supporting Information). The spectra are normalized to show the intensity ratio among the different peaks and nonnormalized spectra can be found in Figure S3a, Supporting Information. With increasing N_2 flow rate, Al-vacancy related defect emission (I_3) becomes dominant, compared to Mg-acceptor related emission (I_2) (Figure S3b, Supporting Information). This observation is consistent with that measured for nondoped AlN, shown in Figure 2b.

To achieve efficient current conduction of p-type AlN, a large concentration of Mg dopants is required. We have subsequently investigated the effect of Mg concentration on the

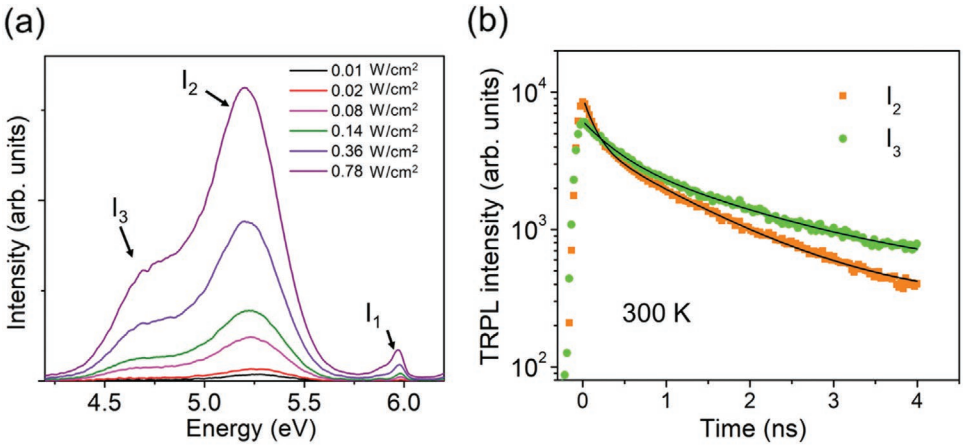

Figure 3. a) Photoluminescence spectra of Mg-doped AlN nanowires measured under different excitation powers. The sample was grown under a substrate temperature of 865 °C, N_2 flow rate of 1 sccm, and Mg BEP of 7×10^{-9} Torr. b) Time-resolved photoluminescence transients of I_2 and I_3 at 300 K. The black curves are fitting results using a single exponential decay.

photoluminesence properties of AlN. Samples in Group C consist of Mg-doped AlN grown under the same substrate temperature of 810 °C and N_2 flow rate of 0.4 sccm but with Mg BEP varied from 1×10^{-9} to 7×10^{-9} Torr. Shown in Figure 2d, Mg-acceptor related emission (I_2) intensity shows an increasing trend with Mg concentration, followed by a decrease for high Mg BEP (≈7×10^{-9} Torr). This suggests enhanced defect formation at very high Mg concentrations, including the increased formation of Al-vacancy related defects, since the incorporated Mg dopants may get desorbed during the growth process as a result of weak Mg–N bond, which leaves vacancies on the cation site.[35] This is further verified by the monotonic increase of Al-vacancy related defect emission (I_3) with increasing Mg concentration, shown in Figure 2d.

To further elucidate the nature of I_2 and I_3 emissions, power-dependent and time-resolved photoluminesence measurements were performed on the sample grown under a substrate temperature of 865 °C, N_2 flow rate of 1 sccm, and Mg BEP of 7×10^{-9} Torr. The growth parameters were chosen such that I_2 emission dominates the PL spectra, which facilitates measurements with large variations of excitation power. The Mg concentration is estimated ≈5×10^{19} cm^{-3}, or higher, based on secondary-ion mass spectrometry (SIMS) studies (Figure S4, Supporting Information). The photoluminescence spectra were analyzed with multiple Gaussian profiles as shown in Figure S5, Supporting Information. With increasing excitation power, I_2 shifts from 5.28 to 5.21 eV, and I_3 shifts from 4.86 to 4.8 eV, shown in **Figure 3**a. This redshift cannot be explained by the DAP related transitions reported for AlN epilayers, which were characterized by a blueshift with increasing excitation intensity.[18] The redshift measured in this study is attributed to a combination of laser-induced heating effect and bandgap renormalization,[36] which were observed in GaN/AlN quantum dots[37] and GaN nanoparticles.[38] Moreover, DAP emissions generally show a slow decay with typical lifetimes in the µs range,[14] whereas I_2 and I_3 decay fast at 300 K, approaching an exponential law with very short lifetimes of 140 and 360 ps, respectively, shown in Figure 3b. Since I_2 and I_3 decay is nearly four orders of magnitude faster than for DAP, both I_2 and I_3 emissions must originate from the transitions involving the conduction band and impurity energy levels inside the bandgap, rather than DAP related transitions as reported in Mg-doped AlN epilayers,[14,15] which further confirms that the use of N-rich conditions can effectively suppress the formation of donor related compensating defects. This observation also explains the high hole concentrations (up to 6×10^{17} cm^{-3}) measured at 300 K in Mg-doped AlN nanowires grown under N-rich conditions.[39] For comparison, hole concentrations ≈2.5×10^{15} cm^{-3} were previously measured in Mg-doped AlN epilayers in spite of the very high measurement temperature (850 K) and the very large Mg concentration (≈10^{20} cm^{-3}).[14]

Previously reported planar *c*-plane AlN LEDs had a turn-on voltage ≈30 V.[1] With optimized growth conditions, we have subsequently investigated the electrical characteristics of AlN nanowire LEDs. The schematic illustration of the device structure is shown in Figure S6a, Supporting Information. Detailed growth conditions and device fabrication process are described in the Experimental Section. The Si doping concentration in n-AlN is ≈1.5×10^{19} cm^{-3} and Mg concentration in p-AlN is estimated in the range of 1×10^{19} to 6×10^{19} cm^{-3}. It is worth noting that introducing Si doping in AlN could shift the fermi level toward conduction band, resulting in a reduced formation energy of Al vacancy in AlN, as shown in Figure 1c. Therefore, we intentionally grew n-AlN and the subsequent unintentionally doped AlN at a relatively high substrate temperature of 875 °C to minimize Al-vacancy related defects. **Figure 4**a shows typical room-temperature *I*–*V* characteristics of as-fabricated AlN nanowire LEDs, which has a small reverse leakage current ≈10 nA at −5 V and strong electroluminescence emission at ≈210 nm (Figure S6b, Supporting Information). Under forward bias, the electrical characteristics exhibit three different trends. Region I is characterized by the presence of a carrier-injection barrier of 2.2 eV related to the large conduction band offset between GaN and AlN (Figure S7, Supporting Information). In Region II, the obtained minimum ideality factor is 4.6 at 2.4 V, but increases drastically with increasing voltage. In Region III, the device shows a turn-on voltage ≈5 V, which is significantly smaller compared with previously reported planar AlN diodes[1]

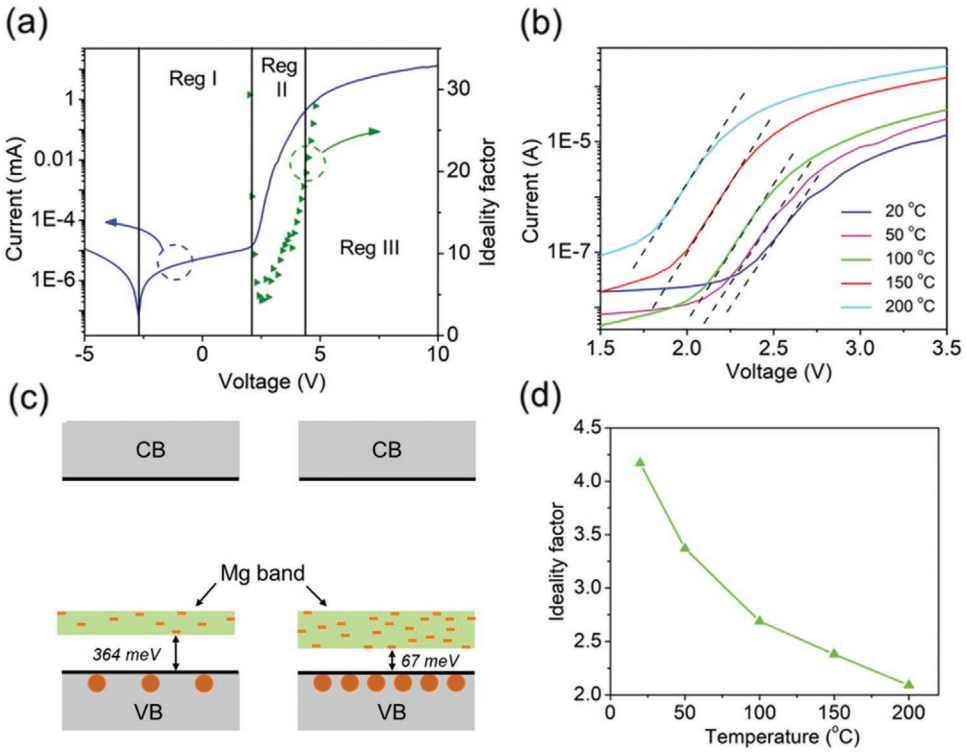

Figure 4. a) *I–V* characteristics of AlN nanowire light emitting diodes (LEDs) measured at room temperature, wherein three regions with different slopes can be identified. b) Temperature-dependent *I–V* characteristics of AlN nanowire LEDs measured in the temperature range of 20–200 °C. c) Illustration of the Mg acceptor energy levels under relatively low (left) and high (right) doping concentrations. The dispersion of Mg acceptor energy levels under very high concentrations can lead to significantly reduced activation energy (right). d) Variations of the minimum ideality factors versus measurement temperature.

and is largely determined by the energy bandgap of AlN. With further increasing voltage, injection current is limited by ohmic potential drop across the diodes. We measured the *I–V* characteristics of AlN LEDs with different Mg doping concentrations. The obtained minimum ideality factor shows a decreasing trend from 14.9 to 3.6 with increasing Mg doping concentrations from approximately 1×10^{19} to 6×10^{19} cm^{-3} (Table SII, Supporting Information). This observation rules out the possibility that the large ideality factors of AlN LEDs are the results of sum of the ideality factors of several rectifying junctions as proposed by Shah et al.[40]

We further performed temperature-dependent *I–V* measurements. Illustrated in Figure 4b, the measured currents between 2.5 and 3.5 V show a monotonic increasing trend with increasing temperature. The dashed black lines in Figure 4b indicate the slopes of forward *I–V*, which are largely invariant from room temperature to 200 °C. The ideality factor, derived by, therefore shows a strong temperature dependence. Previous reports attributed temperature-independent slopes of (log *I*) versus *V* plots to the involvement of charge carrier tunneling.[40–42] The total forward current *J* of the p-i-n diode can be expressed as the sum of diffusion component J_D in the neutral region (both *p* and *n* layers) and the tunneling current J_T in the depletion region,

$$J = J_{D0}\left[\exp\left(\frac{qV_A}{kT}\right)-1\right]+J_{T0}\left[\exp\left(\frac{qV_A}{E_T}\right)-1\right] \quad (1)$$

where is the voltage applied through the AlN p-i-n diode, and is the characteristic tunneling energy.[43,44] Here other factors such as radiative and nonradiative carrier recombination that could lead to larger ideality factors are not considered. Using Equation (1), of 364 meV is obtained for the AlN LED with a Mg concentration of $\approx 1 \times 10^{19}$ cm^{-3}. Values on this order have been attributed to deep level assisted electron (hole) tunneling,[43] such as the deep Mg acceptor levels in AlN, which are in the range of 500–600 meV. In this study, it is observed that decreases to 67 meV for the AlN LED with a Mg concentration of $\approx 6 \times 10^{19}$ cm^{-3}. Very high Mg impurity concentrations in AlN can result in the formation of an impurity band, schematically shown in Figure 4c, instead of localized impurity levels, due to impurity–impurity interactions.[16,39,45] With increasing Mg concentration, the dispersion of Mg acceptor energy levels can lead to reduced ionization energy for a portion of Mg dopants, illustrated in the right panel of Figure 4c. This is consistent with the observation of a reduction of the characteristic tunneling energy from 364 to 67 meV with increasing Mg concentrations from $\approx 1 \times 10^{19}$ to 6×10^{19} cm^{-3}. At elevated temperatures, hole concentrations in the impurity band are increased, and diffusion current becomes more dominant, which leads to a reduction of the ideality factor, shown in Figure 4d. A more detailed analysis of the hole tunneling process is described in Section S9, Supporting Information. The derived value of 67 meV suggests that the ionization energy of Mg dopants can be effectively reduced by

nearly one order of magnitude for AlN nanostructures grown under N-rich epitaxy conditions, compared to that of conventional planar AlN, thereby leading to AlN LEDs with excellent electrical performance.

In summary, through a combined theoretical and experimental study, we show that N-rich epitaxy provides a viable path for achieving efficient p-type conduction of AlN that was not previously possible. The benefits of growing AlN nanostructures under N-rich conditions include: i) suppression of N-vacancy related compensating defect formation, and ii) significant enhancement of Al-substitutional Mg-dopant incorporation. Detailed optical measurements show that Mg-related optical emission originates from conduction-band to Mg-acceptor energy levels, rather than DAP related transition, further confirming the suppressed donor related defect formation under N-rich conditions. Analysis of the current–voltage characteristics of AlN p-i-n diodes suggests that current conduction is dominated by charge carrier (hole) tunneling at room temperature. The characteristic tunneling energy is largely determined by the activation energy of the Mg dopant. At very high Mg concentrations, the dispersion of Mg acceptors leads to drastically reduced activation energy, evidenced by the small tunneling barrier energy of 67 meV. As such, efficient current conduction can be achieved for Mg-doped AlN when grown under N-rich conditions. This study may also offer a path to address the poor current conduction of other ultrawide bandgap semiconductors.

Experimental Section

Molecular Beam Epitaxial Growth: All samples were grown on n-type Si(111) wafer using a Veeco GEN II MBE system equipped with a radio frequency plasma-assisted nitrogen source. AlN(0001) thin films grown under slightly N- and Al-rich conditions at a lower temperature (680 °C) was used to calibrate the Al and N fluxes in AlN-equivalent growth rate units (nm min^{-1}). All samples were grown under ϕ_{Al} = 0.87 nm min^{-1}. N_2 flow rate of 1 sccm corresponds to 12 nm min^{-1} AlN growth rate. Prior to loading into the MBE system, the Si wafer was cleaned using standard solvents and dipped in buffered hydrofluoric acid solution to etch the surface oxide. The AlN nanowire samples in Table 1 were synthesized through two-step experiments. The first step is identical for all samples and consists of the growth of a non-doped GaN nanowire template with ϕ_{Ga} = 0.87 nm min^{-1}. During the second step, ≈150 nm long AlN nanowires were grown at different substrate temperatures, N_2 flow rates, and Mg BEPs. The growth conditions for AlN nanowire-based LEDs include the following steps. Si-doped GaN nanowires (≈100 nm) were first grown at substrate temperature of 780 °C. Si-doped AlN nanowires (≈110 nm) were grown at a substrate temperature of 875 °C. Then, unintentionally doped AlN nanowires of ≈40 nm were grown at the same substrate temperature of 875 °C. The growth was performed under N-rich conditions with the N_2 flow rate of 0.33 sccm during the active region growth. Subsequently, the substrate temperature was reduced to 810 °C and the nitrogen flow rate increases to 0.5 sccm to grow a ≈40 nm Mg-doped p-AlN layer and ≈5 nm p-$Al_{0.2}Ga_{0.8}N$ contact layer. p-$Al_{0.2}Ga_{0.8}N$ contact layer and p-AlN layer were grown at same Mg BEPs. The estimated Si concentration in n-AlN was ≈1.5×10^{19} cm^{-3} and Mg concentration in p-AlN ranges from 1×10^{19}–6×10^{19} cm^{-3}, depending on the Mg flux during the growth.

Structural Characterization: The structure of AlN nanowire p-i-n LED was characterized using double aberration-corrected JEOL JEM3100R05 TEM operated at 300 kV. The nanowires were mechanically removed from Si substrate and dispersed on a lacey carbon film mesh Cu TEM grid. Atomic-resolution, atomic-number sensitive (Z-contrast) STEM high-angle annular dark-field (HAADF) images were obtained using a detector angular range of 63.8–200 mrad.

Photoluminescence Measurements: Photoluminescence measurements were carried out using a 193 nm ArF excimer laser with a repetition frequency of 200 Hz and pulse duration of ≈7 ns. A UV neutral density filter was used to adjust the laser excitation power. The emitted light was collected and spectrally resolved by a high-resolution spectrometer and detected by a liquid nitrogen cooled charge coupled device (CCD). Time-resolved photoluminescence measurements were performed with 200 nm UV laser excitation provided by the fourth harmonic output of a Ti:sapphire laser with a repetition frequency of 80 MHz and pulse duration of 70 fs. A high-speed single photon counter with a temporal resolution of 50 ps was used for the detection of transient signals from time-resolved photoluminescence measurements.

Fabrication of AlN Nanowire-Based LEDs: The AlN p-i-n LEDs were fabricated using standard optical lithography and contact metallization techniques. Ti (80 nm)/Au (20 nm) was deposited on the backside of Si substrate to serve as the n-metal contact. p-Metal contact consisting of Ni (10 nm)/Au (10 nm) was deposited using a tilting angle deposition technique, which also defines the device area in the range of 300 × 300 µm to 1 × 1 mm. Finally, the backside of Si substrate was bonded to an Al plate using conductive silver paste prior to electrical measurements.

Device Characterization: The temperature-dependent *I–V* characteristics of AlN p-i-n LEDs were measured using a Keithley SMU 2400 source meter. The emitted light was collected by an extreme solarization-resistant fiber and spectrally resolved by a high-resolution spectrometer and detected by a CCD.

Supporting Information

Supporting Information is available from the Wiley Online Library or from the author.

Acknowledgements

The work was supported by US Army Research Office under Contract (W911NF-17-1-0109), National Science Foundation Grant DMR-1807984 and DMR-0723032 (for the JEOL JEM 3100R05 AEM), the University of Michigan College of Engineering Blue Sky Research Program, and the technical support from the Michigan Center for Materials Characterization. The DFT calculations used resources of the National Energy Research Scientific Computing (NERSC) Center, a Department of Energy Office of Science User Facility supported under Contract No. DEAC0205CH11231.

Conflict of Interest

Some intellectual property related to this work was licensed to NS Nanotech Inc., which was co-founded by Z.M.

Keywords

aluminum nitride, defects, light emitting diodes, nanostructures, optoelectronics, ultraviolet optoelectronics

Received: April 2, 2020
Revised: May 28, 2020
Published online: August 17, 2020

[1] Y. Taniyasu, M. Kasu, T. Makimoto, *Nature* **2006**, *441*, 325.
[2] Y. Wu, X. Liu, P. Wang, D. A. Laleyan, K. Sun, Y. Sun, C. Ahn, M. Kira, E. Kioupakis, Z. Mi, *Appl. Phys. Lett.* **2020**, *116*, 013101.
[3] D. A. Laleyan, S. Zhao, S. Y. Woo, H. N. Tran, H. B. Le, T. Szkopek, H. Guo, G. A. Botton, Z. Mi, *Nano Lett.* **2017**, *17*, 3738.
[4] J. D. Caldwell, I. Aharonovich, G. Cassabois, J. H. Edgar, B. Gil, D. N. Basov, *Nat. Rev. Mater.* **2019**, *4*, 552.
[5] S. J. Pearton, F. Ren, M. Tadjer, J. Kim, *J. Appl. Phys.* **2018**, *124*, 220901.
[6] H. Umezawa, *Mater. Sci. Semicond. Process.* **2018**, *78*, 147.
[7] S. Hwang, M. Islam, B. Zhang, M. Lachab, J. Dion, A. Heidari, H. Nazir, V. Adivarahan, A. Khan, *Appl. Phys. Express* **2011**, *4*, 012102.
[8] V. Adivarahan, A. Heidari, B. Zhang, Q. Fareed, S. Hwang, M. Islam, A. Khan, *Appl. Phys. Express* **2009**, *2*, 102101.
[9] M. Nami, A. Rashidi, M. Monavarian, S. Mishkat-Ul-Masabih, A. K. Rishinaramangalam, S. R. J. Brueck, D. Feezell, *ACS Photonics* **2019**, *6*, 1618.
[10] M. Monavarian, A. Rashidi, D. Feezell, *Phys. Status Solidi A* **2018**, *216*, 1800628.
[11] Z. Mi, S. Zhao, S. Y. Woo, M. Bugnet, M. Djavid, X. Liu, J. Kang, X. Kong, W. Ji, H. Guo, Z. Liu, G. A. Botton, *J. Phys. D: Appl. Phys.* **2016**, *49*, 364006.
[12] Y. Wu, Y. Wang, K. Sun, Z. Mi, *J. Cryst. Growth* **2019**, *507*, 65.
[13] K. B. Nam, M. L. Nakarmi, J. Li, J. Y. Lin, H. X. Jiang, *Appl. Phys. Lett.* **2003**, *83*, 878.
[14] M. L. Nakarmi, N. Nepal, C. Ugolini, T. M. Altahtamouni, J. Y. Lin, H. X. Jiang, *Appl. Phys. Lett.* **2006**, *89*, 152120.
[15] M. L. Nakarmi, N. Nepal, J. Y. Lin, H. X. Jiang, *Appl. Phys. Lett.* **2009**, *94*, 091903.
[16] A. Pandey, X. Liu, Z. Deng, W. J. Shin, D. A. Laleyan, K. Mashooq, E. T. Reid, E. Kioupakis, P. Bhattacharya, Z. Mi, *Phys. Rev. Mater.* **2019**, *3*, 053401.
[17] Q. Yan, A. Janotti, M. Scheffler, C. G. Van de Walle, *Appl. Phys. Lett.* **2014**, *105*, 111104.
[18] T. Koppe, H. Hofsäss, U. Vetter, *J. Lumin.* **2016**, *178*, 267.
[19] A. M. Siladie, G. Jacopin, A. Cros, N. Garro, E. Robin, D. Caliste, P. Pochet, F. Donatini, J. Pernot, B. Daudin, *Nano Lett.* **2019**, *19*, 8357.
[20] S. Zhao, B. H. Le, D. P. Liu, X. D. Liu, M. G. Kibria, T. Szkopek, H. Guo, Z. Mi, *Nano Lett.* **2013**, *13*, 5509.
[21] W. Guo, M. Zhang, A. Banerjee, P. Bhattacharya, *Nano Lett.* **2010**, *10*, 3355.
[22] S. Zhao, A. T. Connie, M. H. Dastjerdi, X. H. Kong, Q. Wang, M. Djavid, S. Sadaf, X. D. Liu, I. Shih, H. Guo, Z. Mi, *Sci. Rep.* **2015**, *5*, 8332.
[23] N. Sanders, D. Bayerl, G. Shi, K. A. Mengle, E. Kioupakis, *Nano Lett.* **2017**, *17*, 7345.
[24] A. Das, J. Heo, M. Jankowski, W. Guo, L. Zhang, H. Deng, P. Bhattacharya, *Phys. Rev. Lett.* **2011**, *107*, 066405.
[25] S. Zhao, M. Djavid, Z. Mi, *Nano Lett.* **2015**, *15*, 7006.
[26] S. Matta, J. Brault, M. Korytov, T. Q. Phuong Vuong, C. Chaix, M. Al Khalfioui, P. Vennéguès, J. Massies, B. Gil, *J. Cryst. Growth* **2018**, *499*, 40.
[27] K. B. Nam, M. L. Nakarmi, J. Li, J. Y. Lin, H. X. Jiang, *Appl. Phys. Lett.* **2003**, *83*, 2787.
[28] R. Boger, M. Fiederle, L. Kirste, M. Maier, J. Wagner, *J. Phys. D: Appl. Phys.* **2006**, *39*, 4616.
[29] Q. Wang, S. Zhao, A. T. Connie, I. Shih, Z. Mi, T. Gonzalez, M. P. Andrews, X. Z. Du, J. Y. Lin, H. X. Jiang, *Appl. Phys. Lett.* **2014**, *104*, 223107.
[30] S. Fernandez-Garrido, J. K. Zettler, L. Geelhaar, O. Brandt, *Nano Lett.* **2015**, *15*, 1930.
[31] J. Ristić, E. Calleja, S. Fernández-Garrido, L. Cerutti, A. Trampert, U. Jahn, K. H. Ploog, *J. Cryst. Growth* **2008**, *310*, 4035.
[32] T. Zywietz, J. Neugebauer, M. Scheffler, *Appl. Phys. Lett.* **1998**, *73*, 487.
[33] K. Kishino, S. Ishizawa, *Nanotechnology* **2015**, *26*, 225602.
[34] K. Yamano, K. Kishino, *Appl. Phys. Lett.* **2018**, *112*, 091105.
[35] Y. H. Liang, E. Towe, *Appl. Phys. Rev.* **2018**, *5*, 011107.
[36] M. Kira, S. W. Koch, *Semiconductor Quantum Optics*, Cambridge University Press, Cambridge, England **2012**.
[37] I. Aleksandrov, K. Zhuravlev, *Phys. Status Solidi C* **2010**, *7*, 2230.
[38] A. B. Slimane, A. Najar, R. Elafandy, D. P. San-Roman-Alerigi, D. Anjum, T. K. Ng, B. S. Ooi, *Nanoscale Res. Lett.* **2013**, *8*, 342.
[39] N. H. Tran, B. H. Le, S. Zhao, Z. Mi, *Appl. Phys. Lett.* **2017**, *110*, 032102.
[40] J. M. Shah, Y. L. Li, T. Gessmann, E. F. Schubert, *J. Appl. Phys.* **2003**, *94*, 2627.
[41] P. Perlin, M. Osiński, P. G. Eliseev, V. A. Smagley, J. Mu, M. Banas, P. Sartori, *Appl. Phys. Lett.* **1996**, *69*, 1680.
[42] H. C. Casey, J. Muth, S. Krishnankutty, J. M. Zavada, *Appl. Phys. Lett.* **1996**, *68*, 2867.
[43] K. B. Lee, P. J. Parbrook, T. Wang, J. Bai, F. Ranalli, R. J. Airey, G. Hill, *Phys. Status Solidi B* **2010**, *247*, 1761.
[44] M. Lee, H. Lee, K. M. Song, J. Kim, *Nanomaterials* **2018**, *8*, 543.
[45] A. T. Connie, S. Zhao, S. M. Sadaf, I. Shih, Z. Mi, X. Du, J. Lin, H. Jiang, *Appl. Phys. Lett.* **2015**, *106*, 213105.